PCCP

Accepted Manuscript

ROYAL SOCIETY OF CHEMISTRY

www.rsc.org/pccp

Cite this: DOI: 10.1039/c0xx00000x

www.rsc.org/xxxxxx

ARTICLE TYPE

Spatial Dispersion of Lone Electron Pairs? – Experimental Charge Density of Cubic Arsenic(III) Oxide

Piotr A. Guńka,*[a] Zygmunt Gontarz[a] and Janusz Zachara[a]

Received (in XXX, XXX) Xth XXXXXXXXX 20XX, Accepted Xth XXXXXXXXX 20XX

DOI: 10.1039/b000000x

The first experimental charge density study of arsenolite, cubic polymorph of arsenic(III) oxide, extended by periodic DFT calculations is reported. The presence of weak As···O interactions is confirmed and their topological characterization based on experimental electron density is provided. Spatial dispersion of arsenic lone electron pair into three domains is observed in the Laplacian of electron density as well as in electron localization function. It results from the clustering of As atomic cores in the crystal structure and/or from the presence of strong As−O bonds. Similar phenomenon is recognized in the crystal structures of antimonates(III) and bismutates(III) of alkaline metals indicating this could be a more general feature worth of further investigations.

Introduction

Despite being notably weaker than covalent or ionic bonds, non-covalent interactions play a significant role in the chemical world. Hydrogen bonds are probably the most well-known example of this, being responsible for holding DNA strands together or causing remarkable properties of water. But there are many more types of weak directional interactions which hold molecules together in crystals such as C−H···O,[1] C−H···π,[2] halogen[3] or chalcogen bonds[4]. Arsenic···oxygen interactions present in arsenic(III) compounds are yet another example of them. It was noted by Pertlik that oxygen atoms which surround arsenic atomic cores may be divided into two groups. The first one includes the so-called primary ligands with As−O bond length of around 1.8 Å and the second one consists of oxygen atoms located 2.7−3.4 Å away from arsenic atoms, 3.37 Å being the sum of As and O van der Waals radii[5]. The secondary ligands are located approximately in the *trans* positions with respect to the primary ones which could indicate that they are an example of donor-acceptor interactions.[6,7] The significance of the interactions is evidenced by the differences in the crystal packing of phosphorus(III) oxide, arsenolite and senarmontite, the cubic polymorphs of arsenic(III) and antimony(III) oxides, respectively. In the latter two As_4O_6 and Sb_4O_6 molecules are surrounded by 4 neighbours in a face-to-face fashion which results in a structure with molecules' barycentres forming a 3D diamond net (Fig. 1).[8–10] On the other hand, P_4O_6 molecules of phosphorus(III) oxide crystallize in the monoclinic crystal system. Every molecule has only two neighbours in a face-to-face orientation analogous to that found in arsenolite and senarmontite. This leads to the formation of zig-zag chains along the *Y* axis that are packed in a deformed "honeycomb manner".[11] Gibbs and co-workers computed charge density distribution in arsenic oxides and analysed its topological properties within the QTAIM framework.[12] Their work reported topological description of As···O, As···As and O···O bond paths attributing them to As···O, As···As and O···O interactions. There is an experimental charge density study of senarmontite,[10] cubic antimony(III) oxide polymorph, which makes it appealing to try to extend the study to arsenic(III) oxide and even phosphorus(III) oxide.

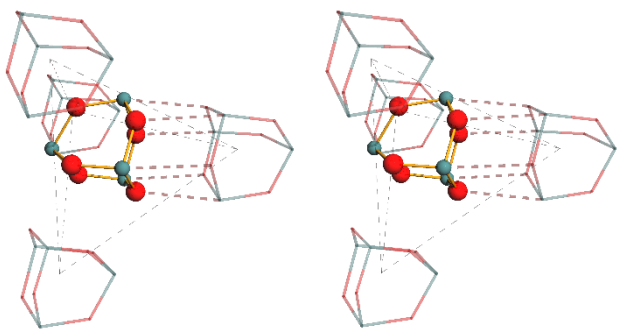

Fig. 1 Stereo view of tetrahedral molecular surrounding of an As_4O_6 molecule in arsenolite. As···O interactions are depicted as brown dashed lines for one of the intermolecular face-to-face contact. Grey dashed lines connect barycenters of central molecule's closest neighbours, forming a tetrahedron. Arsenic and oxygen atoms are coloured green and red, respectively.

This and the fact that there has been no experimental charge density study of As_2O_3 have led us to undertake such investigations, beginning with the cubic polymorph – arsenolite. Herein, we present experimental and theoretical study of electron density distribution (EDD) in arsenolite using the Hansen-Coppens multipolar model (MM).[13] The topological features of the resulting EDD are described and analysed in terms of the Bader's Quantum Theory of Atoms in Molecules (QTAIM)[14], electron localisation function (ELF)[15–17] and non-covalent interactions (NCI) descriptor based on reduced density gradient (RDG)[18,19]. The aim of the study is twofold; namely, to study weak directional As···O interactions and to investigate how the stereoactivity of arsenic lone electron pair (LEP) is affected by intermolecular interactions.

Methodology

Crystallisation and X-ray Diffraction

Charge-density-quality arsenolite single crystals were grown via slow ammonium arsenite decomposition from diluted aqueous solution accompanied by water evaporation.[20] X-ray diffraction data were collected at 100(2) K with graphite-monochromated Mo-Kα radiation on the Agilent Technologies κ-CCD Gemini A Ultra diffractometer. Cell refinement and data collection as well as data reduction and analysis were performed with the CrysAlis^{PRO} software,[21] whereas data merging was carried out with SORTAV.[22] Full details on the measurement and the data processing information are given in the footnote‡ and in the Supporting Information.

Theoretical structure factors computations

Theoretical structure factors (SFs) were obtained from periodic DFT computations using the Wien2k program where linearized augmented plane wave + local orbitals (LAPW+lo) method is implemented.[23] Calculations were carried out at the experimental geometry without relaxation using the PBE functional[24,25] and a 17x17x17 *k*-point mesh. The RK_{max} and G_{max} parameters were set to 10 and 16, respectively, and spherical harmonics with *l* up to 10 were used in the wavefunction within atomic spheres. Muffin tin radii of 0.937 Å and 0.847 Å were utilized for arsenic and oxygen, respectively. The SCF convergence threshold on energy was set to 0.0001 Ry (0.0014 eV). The ED was analyzed with the AIM module of Wien2k and with the Critic2 program[26,27] which was also used for the analysis of the ED Laplacian.[28]

Multipole refinements

Independent atom model (IAM) refinements were carried out using SHELXL-2014[29] whereas multipolar refinements and the topological analysis of the resulting ED were carried out in the XD2006 program[30] utilizing the Hansen-Coppens model[13]. In the model electron density is divided into contributions from pseudoatoms with the following partitioning of electron density for individual pseudoatoms:

$$\varrho(r) = P_c\varrho_{core}(r) + P_v\kappa^3\varrho_{val}(\kappa r) + \sum_{l=0}^{lmax}\kappa'^3 R_l(\kappa' r)\sum_{m=0}^{l} P_{lm\pm}\, d_{lm\pm}(\theta,\varphi) \quad (1)$$

where $\varrho_{core}(r)$ is the spherical atomic core density with a population of P_c electrons (normally not refined), $\varrho_{val}(\kappa r)$ is the spherical valence electron density with a contraction factor κ and population P_v and the asphericity of valence electron density is expressed in terms of real spherical harmonics $d_{lm\pm}(\theta,\varphi)$ with populations $P_{lm\pm}$ and Slater-type radial functions $R_l(\kappa' r)$ with contraction parameter κ'.

All symmetry-allowed multipole populations up to hexadecapole and octupole level for arsenic and oxygen atoms, respectively, were refined. The aspherical atom models employed scattering factors derived from STO relativistic wave functions found in the VM data bank of XD2006. At first scale factor, atomic positions and anisotropic displacement parameters were refined. Then multipole populations were refined in a stepwise manner and afterwards all parameters including κ's for both atoms and κ' for arsenic atom only were refined together. Anharmonic thermal motion of arsenic was described using Gram-Charlier coefficients up to fourth order which led to the removal of the Shashlik-like residual density around arsenic atom (see Fig. S1 in the SI). Extinction correction had to be included in the model and the type I correction with Gaussian mosaic spread was found to perform best.[31,32] Refinements were carried out against *F* and only reflections for which $F/\sigma(F) > 2$ and $\sin\theta/\lambda < 1.125$ Å^{-1} were used together with statistical weights ($1/\sigma^2(F)$). More details on the refinement strategy and on the refinement quality analysis are given in Table 2 as well as in the Supporting information (Table S1 and Fig. S4 and S5). The modelling of charge density with the multipolar model resulted with fits of satisfactory quality. The model is referred to as exp_MM later on. The highest peak and hole in the residual density are −0.44 and +0.66 e·Å^{-3}, respectively. The highest residual density is located on the As atomic core. Most of the highest peaks as well as the deepest hole are all situated on the threefold symmetry axis which agrees with the observation that experimental noise tends to accumulate along high-symmetry axes (see Fig. S1).[33] Complete list of peaks and holes in the residual density is given in Table S2.

Table 2 Multipole refinement details

	Theory (W2k_MM)	Experiment (exp_MM)
R(F)	0.17%	0.71%
R_w(F)	0.19%	1.26%
GOF	3.35	0.97
N_{refl}	429	428
$\Delta\rho_{min}$/ $\Delta\rho_{max}$ /eÅ^{-3}	−0.21/+0.27	−0.44/+0.66

The ED resulting from multipolar refinements was used to calculate ELF using the XD2006 program and served as a basis for the computations of RDG-based NCI descriptors carried out by the NCImilano code[34]. The resulting properties were visualized by the MolIso program.[35]

Results

Crystal structure of arsenolite

The crystal structure of arsenolite has been known for over 90 years now.[9,36–39] It crystallizes in the $Fd\bar{3}m$ (origin choice 2) space group with one arsenic and one oxygen atom in the asymmetric unit. The adamantane-like As_4O_6 molecule occupies the 8*b* special position of $4\bar{3}m$ point group symmetry. The As−O bond length determined from IAM refinement equals 1.79616(19) Å and the As···O separation between neighbouring molecules is 3.0052(3) Å which is significantly less than the sum of As and O van der Waals radii (3.37 Å).[5]

Topological parameters of ED

The analysis of ED topological properties yields information about chemical bonds and weak interactions. For instance, by looking at the bond paths and ED as well as Laplacian of ED at the bond critical point (BCP), a point on the bond path where ED reaches minimum, one may assess the character of an interaction. The topological descriptors of BCPs found in the crystal structure of arsenolite are summarized in Table 3. The positive value of $\nabla^2\rho$ and relatively high value of ρ at the As−O BCP indicate that this is an interaction of intermediate type between closed-shell and shared which points to a significant ionic contribution to the

Cite this: DOI: 10.1039/c0xx00000x

www.rsc.org/xxxxxx

ARTICLE TYPE

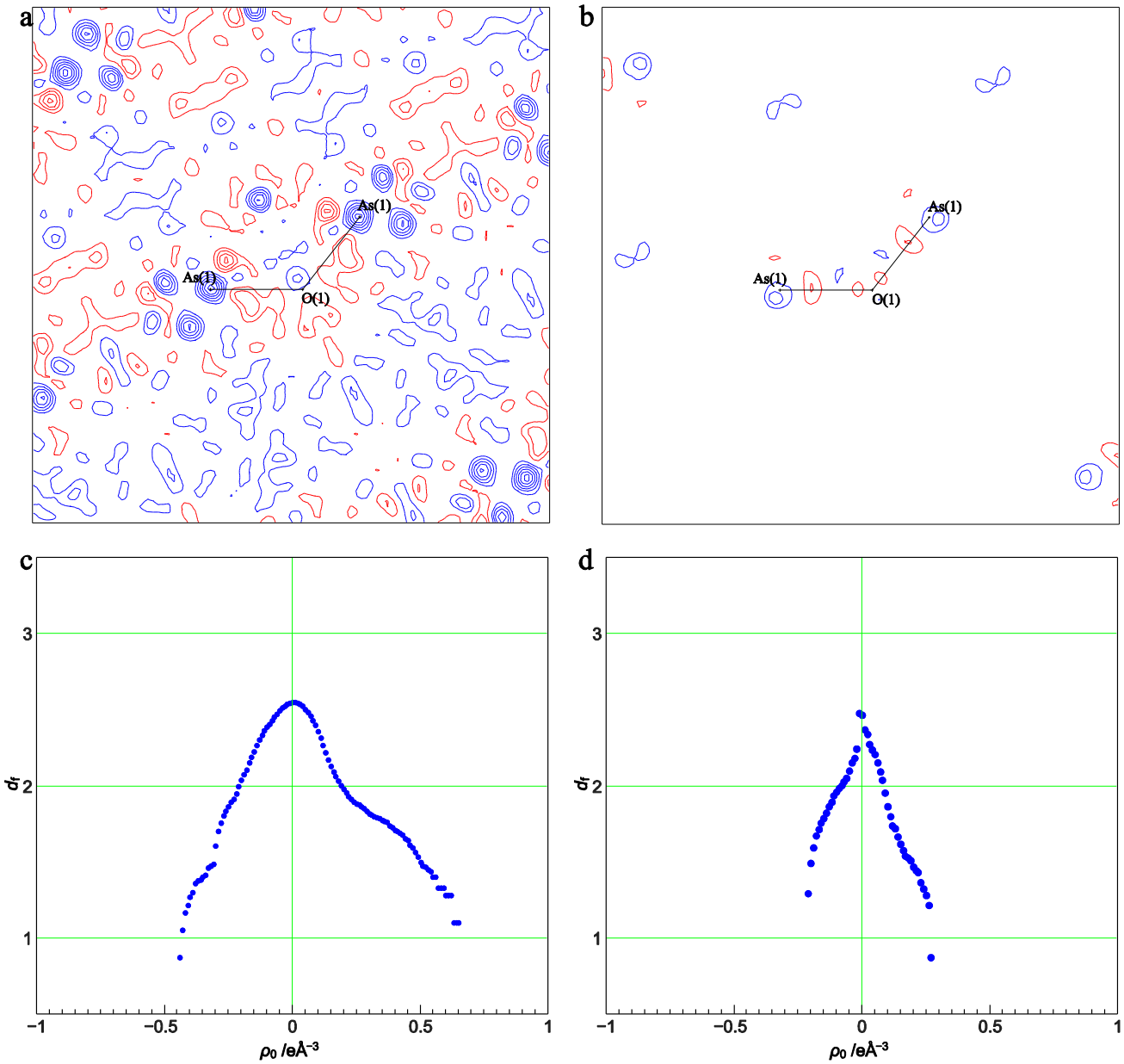

Fig. 2 Residual electron density map in the As−O−As plane resulting from the exp_MM (a) and W2k_MM (b) models as well as fractal dimensions of the residual electron density. Fit against (c) experimental and (d) theoretical SFs. Contours at 0.1 eÅ^{-3}; blue solid lines – positive, red solid lines – negative values.

covalent As−O bond. This is confirmed by the values of net charges of +2.45 and −1.62 on arsenic and oxygen atoms, respectively.

The presence of weak As···O interactions has been confirmed experimentally for the first time using the QTAIM method. The ρ_{BCP} value slightly higher than derived from *ab initio* computations whereas the $\nabla^2\rho_{BCP}$ is slightly lower. It can be concluded that the strength of the interactions is a little underestimated *in silico*. Basing on the exp_MM EDD, RDG-NCI descriptor was calculated for two interacting As_4O_6 molecules in order to assess the character of the As···O and O···O intermolecular interactions. The 0.3 RDG isosurfaces are plotted with $\rho \cdot \mathrm{sign}(\lambda_2)$ (NCI descriptor) and with approximate total energy density obtained using Abramov's functional mapped onto them in Fig. 3 (see animations in the SI for a better glimpse of RDG spatial distribution).[40] The RDG isosurface for As_4O_6 dimer exhibits separate regions

corresponding to As···O and O···O BCPs. The NCI-descriptor is negative in the vicinity of As···O BCP while for the O···O interactions the NCI-descriptor is negative very close to the BCP and changes to positive further away from it. Moreover, the regions around As···O and O···O BCPs differ in the sign of the total energy densities on the 0.3 RDG isosurfaces *i.e.* the energy density associated with As···O interactions is negative while for the O···O interactions it is positive.

Table 3 The topological properties of ED at the bond critical points in the arsenolite structure. Electron density, the Laplacian of electron density and ellipticity at the bond critical point are denoted ρ_{BCP}, $\nabla^2\rho_{BCP}$ and ε, respectively.

Bond path	model	exp_MM	W2k_MM	Wien2k[a]	Ref. 12
As−O	ρ_{BCP}/ e·Å^{-3}	1.044	1.059	1.003	0.989
	$\nabla^2\rho_{BCP}$/ e·Å^{-5}	8.438	5.948	7.372	7.873
	ε	0.0	0.0	0.0	0.0
	d_{As-O} /Å	1.7948(3)	1.795	1.795	1.786
	$d_{As\cdots BCP}$ /Å	0.842	0.895	0.871	-
	$d_{O\cdots BCP}$ /Å	0.954	0.900	0.924	-
As···O	ρ_{BCP}/ e·Å^{-3}	0.109	0.087	0.085	0.085
	$\nabla^2\rho_{BCP}$/ e·Å^{-5}	0.720	0.904	0.926	0.928
	ε	0.0	0.1	0.0	0.1
	$d_{As\cdots O}$ /Å	3.0062(4)	3.006	3.006	3.050
	$d_{As\cdots BCP}$ /Å	1.640	1.587	1.60	-
	$d_{O\cdots BCP}$ /Å	1.409	1.427	1.447	-
O···O	ρ_{BCP}/ e·Å^{-3}	0.072	0.076	0.072	0.073
	$\nabla^2\rho_{BCP}$/ e·Å^{-5}	1.047	0.888	0.969	0.912
	ε	7	9	763	4
	$d_{O\cdots O}$ /Å	2.9866(2)	2.987	2.987	3.022
	$d_{O\cdots BCP}$ /Å	1.499	1.495	1.493	-
	$d_{O\cdots BCP}$ /Å	1.495	1.493	1.493	-

[a] results of direct analysis of EDD computed with the AIM module of the Wien2k program suite.

Lone electron pairs (LEPs)

The analysis of the negative Laplacian of ED allows one to find regions of charge concentration and depletion. In particular, (3,−3) critical points in $-\nabla^2\rho$ correspond to the so-called charge concentrations which, when located in the valence region of an atom, are called valence-shell charge concentrations (VSCCs) and correspond to bonding and non-bonding electrons. However, they cannot always be treated as one-to-one representation of Lewis electron pairs.[41] The analysis of negative Laplacian of ED obtained in the exp_MM model reveals maximum on each As−O bond located very close to oxygen atom and a maximum in the As−O−As plane on the bisector of the As−O−As convex angle. Interestingly, there are also three maxima around the vertex of arsenic ψ-tetrahedron where LEP is located, indicating three VSCCs in this region (see Fig. 4 and Table 4). This suggests that the LEP of arsenic atom is dispersed into three distinct regions of space. The effect is also present in the ED from the W2k_MM model albeit far less pronounced. What is intriguing is that direct topological analysis of EDD Laplacian calculated in Wien2k yields no VSCCs around arsenic atom. Another difference between exp_MM and W2k_MM models is that there are two VSCCs around oxygen instead of the one lying on the As−O−As angle bisector $-\nabla^2\rho$ in addition to the VSCCs on the As−O bonds (cf. Fig. 4a).

Electron localisation function (ELF) was computed using the XDPROP module of XD2006 program for a cluster As_4O_6 molecules surrounding the LEP of interest. The cluster incorporated three arsenolite molecules interacting via As···O interactions with the As in question and three additional molecules with As···As distances of 4.5500(1) Å (see animations of ELF in the SI for the cluster visualisation). The "dispersion" of LEPs is present in the ELF for both models as evidenced by three attractors located *trans* with respect to the primary As−O bonds (see Fig. 5 and animations in the SI). The domains around attractors are slightly smaller in the W2k_MM than in the exp_MM. Furthermore, the three domains merge into one for ELF = 0.8 in the W2k_MM (see Fig. 5) which happens in case of the exp_MM for ELF = 0.73.

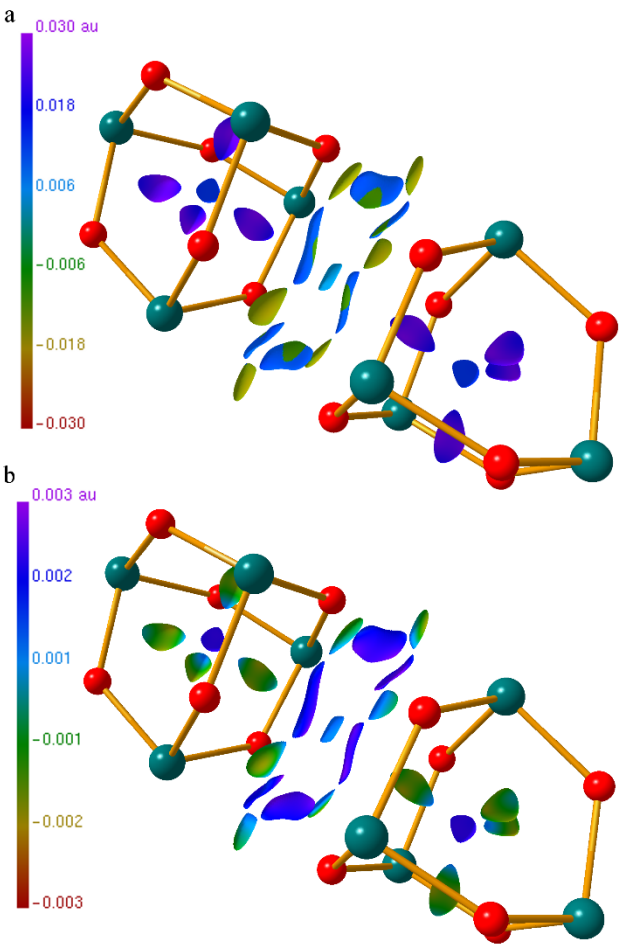

Fig. 3 0.3 RDG for two interacting As_4O_6 molecules in the exp_MM model. RDG was calculated using an ED cutoff of 0.08 e/au to single out only RDG isosurfaces associated to NCI, according to Ref. 18. The function mapped onto isosurface is the NCI descriptor (a) and approximate total energy density obtained using Abramov's functional (b). The colour scale is reported on the left.

Discussion

The topological analysis of the experimental EDD in arsenolite crystal structure led to the first experimental characterization of weak As···O interactions. Similarly as in previous computational study, we have observed O···O bond paths.[12] Their ellipticity value is very high and varies between 4 and 763 (!) , depending on the model. The analysis of NCI using the 0.3 RDG surface

Cite this: DOI: 10.1039/c0xx00000x

www.rsc.org/xxxxxx

ARTICLE TYPE

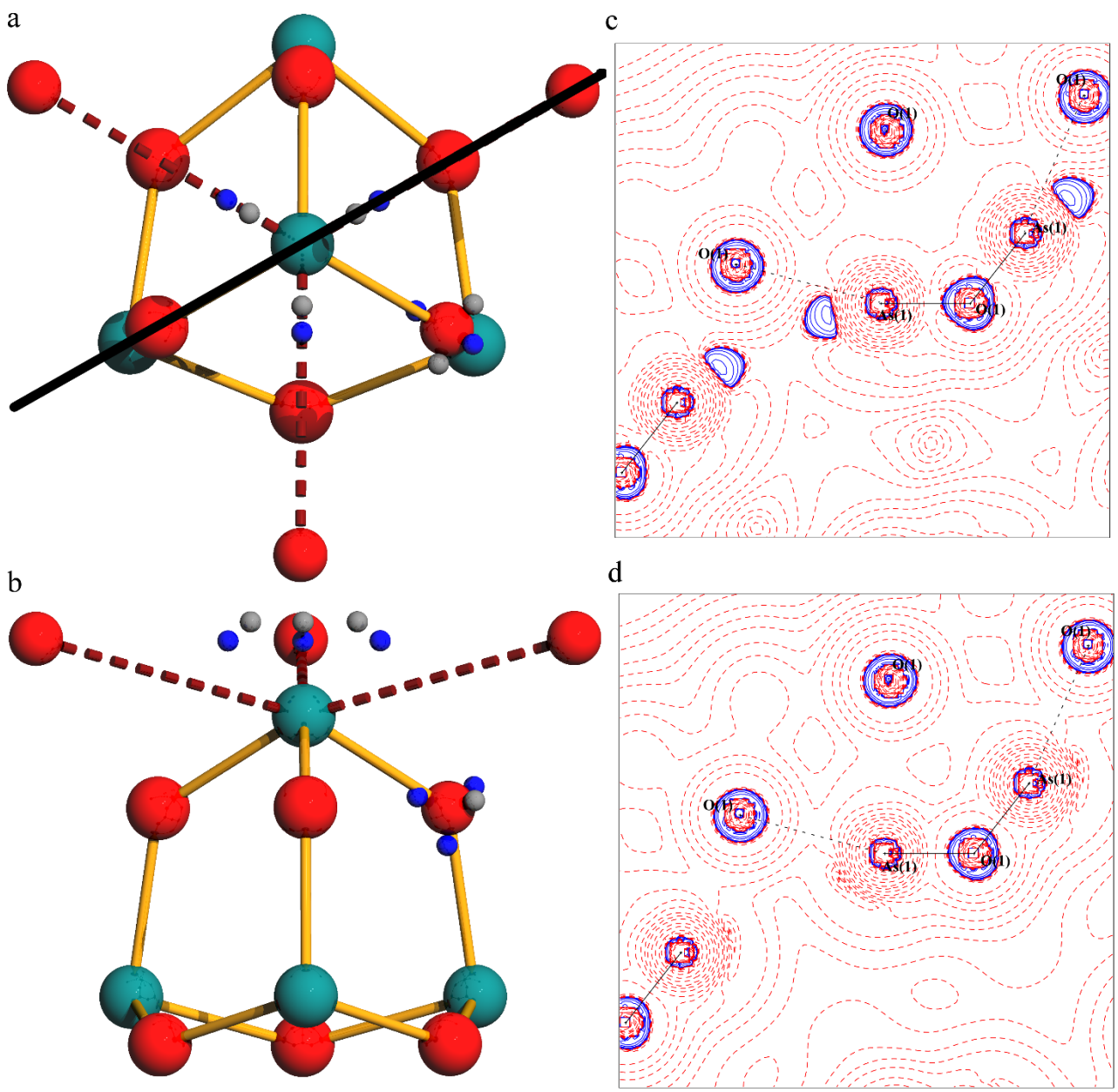

Fig. 4 (3, −3) critical points in the negative Laplacian of ED corresponding to VSCCs. Blue and grey spheres denote CPs in the ED from exp_MM and W2k_MM respectively. Views along (a) and perpendicular to (b) threefold axis are presented. Laplacian of ED in the As−O−As plane, denoted with solid black line in (a), for the exp_MM (b) and W2k_MM (c) models. Blue solid lines indicate negative values and red dashed positive; contour values $\pm 2, 4, 8 \cdot 10^n$ eÅ$^{-5}, n = -3, -2, \ldots, 3, 4$. Dashed lines denote As···O interactions and are drawn as a guide for the eye.

plots reveals separate regions corresponding to As···O and O···O bond paths and the NCI descriptor classifies the As···O interactions as attractive while it is ambiguous for the O···O interactions. It is noteworthy that Whitten and co-workers did not find any O···O bond paths in the crystal structure of senarmontite, cubic form of Sb_4O_6, which is isostructural with arsenolite and where molecules are packed even closer than in arsenolite as demonstrated by the Sb···O separation of 2.9018(9) Å compared to As···O separation of 3.0062(4) Å.[10] It has been recently clearly stated by Foroutan-Nejad and co-workers that the sole detection of a bond path between two atoms is neither necessary nor sufficient for a bonding interaction to be present between them.[42] Moreover, our studies of ammonium polyoxoarsenates(III) and works of Pertlik have shown that weak As···O interactions in the *trans* position with

respect to primary As−O bonds are a structure directing factor in arsenate(III) oxy compounds.[6,43] Summing up, we conclude that it is the As···O interactions which bring about the observed face-to-face arrangement of As_4O_6 molecules. The exact role and nature of O···O interactions lying behind the observed O···O bond paths cannot be determined unambiguously based on our data, but it can certainly be said that their nature is different from As···O interactions as evidenced by different sign of the total energy densities mapped onto RDG isosurfaces associated with the interactions.

Gibbs and co-workers call the observed weak directional interactions van der Waals interactions and try to prove the point that the vdW interactions are indeed directional.[12] We think that this is a matter of semantics and it is beneficial to distinguish between weak directional interactions such as donor-acceptor interactions and non-directional interactions i.e. van der Waals interactions. There is no continuum between van der Waals forces and chemical bonds which is advocated by Gibbs et al.[12] The continuum exists between classical chemical bonds and weak directional interactions in our view.

Table 4 Properties of VSCCs around arsenic atom in the arsenolite structure.

model	$\rho(\mathbf{r}_c)$ / e·Å^{-3}	$\nabla^2\rho(\mathbf{r}_c)$ / e·Å^{-5}	$d_{As\cdots VSCC}$ / Å
exp_MM	0.320	−1.105	1.084
W2k_MM	0.415	0.017	1.055

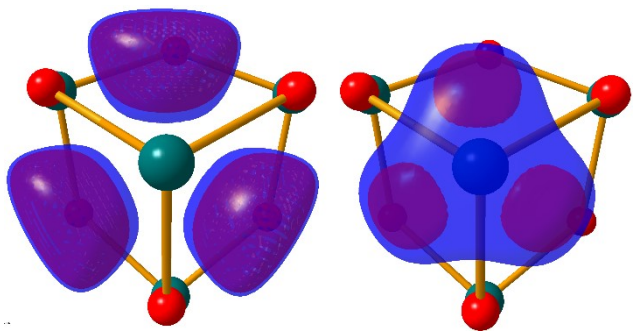

Fig. 5 3D representations of ELF isosurfaces with ELF = 0.9 and 0.8 coloured red and blue, respectively. The exp_MM model shown on the left and W2k_MM on the right side.

To the best of our knowledge the effect of LEP "dispersion" has been described for the first time herein. It may be rationalized using the Brown's bond valence model approach to LEPs. Brown treats their stereoactivity as a direct consequence of the formation of strong chemical bonds by coordination centers and ligands which results from the valence matching rule.[44] LEPs are naturally inactive, but when a coordination center forms strong chemical bonds, LEP is concentrated in one region of the coordination sphere and becomes stereoactive. In case of arsenolite, strong (primary) As−O bonds are formed and bonding ED is localized on one side of the arsenic coordination sphere whereas the non-bonding ED is situated on the opposite side which results in a stereoactive LEP. According to the model, one may expect that three ED concentrations are formed in the *trans* positions with respect to the As−O bonds. These concentrations correspond to three maxima observed in the LEP region in the negative ED Laplacian and to the three attractors in the ELF located around threefold axes. Given that ELF provides a faithful visualisation of the valence shell electron pair repulsion (VSEPR) theory as stated by Becke and Edgecombe,[15] one could also say that it is the repulsion between bonding electrons of As−O bonds and LEP that causes the formation of three separate domains in ELF of arsenic LEP.

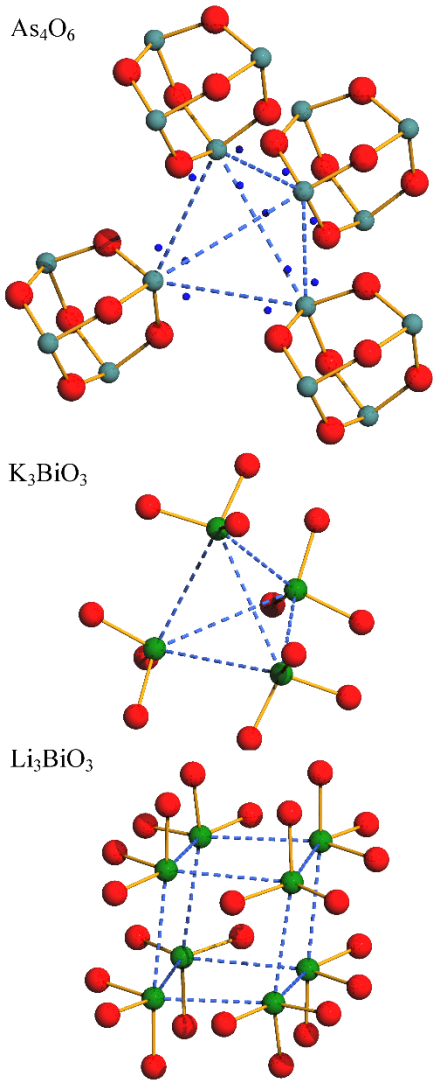

Fig. 6 Tetrahedral cages in the structure of arsenolite as well as examples of tetrahedral and cubic cages made up of bismutate(III) anions in the crystal structures of K_3BiO_3 and Li_3BiO_3, respectively. Small blue spheres denote VSCCs of arsenic atoms in ED obtained from experimental structure factors.

However, there could also be a different reason for the "dispersion" effect of LEPs, namely their clustering. As_4O_6 molecules pack in arsenolite in such a way that As LEPs point towards one another (see Fig. 6) forming tetrahedra of arsenic atomic cores with clustered LEPs. Analogous clustering behavior is present in the structures of cubic Sb_4O_6 (senarmontite)[10] as well as of antimonates(III) and bismutates(III) of alkaline metals. For instance, the crystal structure of Li_3BiO_3 contains $(BiO_3^{3-})_8$ units where Bi atomic cores form a distorted cube[45] whereas the structures of Na_3BiO_3, K_3BiO_3 and Na_3SbO_3 comprise $(XO_3^{3-})_4$ clusters with pnictogen atoms located in the vertices of tetrahedra

(Fig. 6).[46,47] In all the mentioned examples LEPs point towards the center of the clusters and every pnictogen atomic core has three closest neighbors in the cluster. It remains unclear what the driving force of the cages formation is given that clustering of anions is highly unfavorable from the purely electrostatic point of view.

Conclusions

EDD has been determined experimentally for arsenolite single crystal utilising Hansen-Coppens model. The presence of weak directional As···O interactions has been confirmed in experiment for the first time using the QTAIM and RDG-NCI methods. RDG-NCI analysis of intermolecular interactions indicates that As_4O_6 cages are held together by As···O interactions and the exact nature of O···O interactions associated with the observed bond paths cannot be unequivocally determined. Surprising results concerning LEP have been obtained both by the analysis of ED Laplacian and ELF. Arsenic LEPs are dispersed into three domains located *trans* with respect to the primary As−O bonds as evidenced by the analysis of ELF. This could be related to the formation of these chemical bonds and/or to the tetrahedral clustering of arsenic atoms. Similar clustering has been observed in Sb(III) and Bi(III) oxysalts, suggesting LEPs may play significant role in this phenomenon which implies it may be a more general effect and it should be investigated thoroughly. Therefore, further studies using synchrotron X-ray radiation and utilising X-ray wavefunction refinement are under way.

Acknowledgements

The authors thank the National Science Centre for financial support of this work (grant DEC-2012/05/N/ST5/00283). Calculations have been carried out using resources provided by Wroclaw Centre for Networking and Supercomputing (http://www.wcss.pl), grant No. 260.

Notes and references

[a] *Faculty of Chemistry, Warsaw University of Technology, Noakowskiego 3, 00-664 Warsaw, Poland; E-mail: piogun@ch.pw.edu.pl*

† Electronic Supplementary Information (ESI) available: diffraction data collection details, refinement strategy description, refinement quality material including maps and table of maxima and minima in the residual density, graphs comparing theoretical and experimental structure factors, animations of RDG and ELF isosurfaces. See DOI: 10.1039/b000000x/

‡ **Crystal data for arsenolite:** As_4O_6, M = 395.69 g/mol, $a = b = c$ = 11.00003(4) Å, V = 1331.011(15) Å^3, T = 100(2) K, space group $Fd\bar{3}m$, Z = 8, μ(MoKα) = 19.880 mm^{-1}, 39808 reflections measured, 631 independent reflections (R_{int} = 0.0337, R_{sigma} = 0.0121). F(000) = 1440.0. Crystal size 0.096 × 0.080 × 0.034 mm^3. 2θ range for data collection 6.416° to 134.69°. Index ranges $-29 \le h \le 30$, $-28 \le k \le 29$, $-29 \le l \le 30$.

1 G. R. Desiraju and T. Steiner, *The Weak Hydrogen Bond: In Structural Chemistry and Biology*, Oxford University Press, 2001.
2 M. Nishio, M. Hirota and Y. Umezawa, *The CH/π Interaction: Evidence, Nature, and Consequences*, John Wiley & Sons, 1998.
3 P. Metrangolo and G. Resnati, Eds., *Halogen Bonding - Fundamentals and Applications*, Springer Berlin Heidelberg, Berlin.
4 M. E. Brezgunova, J. Lieffrig, E. Aubert, S. Dahaoui, P. Fertey, S. Lebègue, J. G. Ángyán, M. Fourmigué and E. Espinosa, *Cryst. Growth Des.*, 2013, **13**, 3283–3289.
5 A. Bondi, *J. Phys. Chem.*, 1964, **68**, 441–451.
6 F. Pertlik, *Monatshefte für Chemie*, 1979, **110**, 387–392.
7 H. A. Bent, *Chem. Rev.*, 1968, **68**, 587–648.
8 G. V. Gibbs, A. F. Wallace, R. Zallen, R. T. Downs, N. L. Ross, D. F. Cox and K. M. Rosso, *J. Phys. Chem. A*, 2011, **114**, 6550–6557.
9 R. M. Bozorth, *J. Am. Chem. Soc.*, 1923, **45**, 1621–1627.
10 A. E. Whitten, B. Dittrich, M. A. Spackman, P. Turner and T. C. Brown, *Dalton T.*, 2004, 23–29.
11 M. Jansen and M. Moebs, *Inorg. Chem.*, 1984, **23**, 4486–4488.
12 G. V. Gibbs, A. F. Wallace, D. F. Cox, P. M. Dove, R. T. Downs, N. L. Ross and K. M. Rosso, *J. Phys. Chem. A*, 2009, **113**, 736–749.
13 N. K. Hansen and P. Coppens, *Acta Crystallogr. A*, 1978, **34**, 909–921.
14 R. F. Bader, *Atoms in molecules: a quantum theory*, Oxford University Press, Incorporated, 1994.
15 A. D. Becke and K. E. Edgecombe, *J. Chem. Phys.*, 1990, **92**, 5397–5403.
16 A. Savin, R. Nesper, S. Wengert and T. F. Fässler, *Angew. Chem. Int. Ed. Engl.*, 1997, **36**, 1808–1832.
17 V. Tsirelson and A. Stash, *Chem. Phys. Lett.*, 2002, **351**, 142–148.
18 E. R. Johnson, S. Keinan, P. Mori-Sánchez, J. Contreras-García, A. J. Cohen and W. Yang, *J. Am. Chem. Soc.*, 2010, **132**, 6498–6506.
19 G. Saleh, C. Gatti, L. Lo Presti and J. Contreras-García, *Chem. Eur. J.*, 2012, **18**, 15523–15536.
20 P. A. Guńka, M. Dranka, J. Piechota, G. Z. Żukowska, A. Zalewska and J. Zachara, *Cryst. Growth Des.*, 2012, **12**, 5663–5670.
21 *CrysAlisPro Software system ver. 171.37.35*, Agilent Technologies UK Ltd, Oxford, UK, 2014.
22 R. Blessing, *Acta Crystallogr. A*, 1995, **51**, 33–38.
23 P. Blaha, K. Schwarz, G. K. H. Madsen, D. Kvasnicka and J. Luitz, *Wien2k, An Augmented Plane Wave + Local Orbitals Program for Calculating Crystal Properties*, Technische Universität Wien, 2001.
24 J. P. Perdew, K. Burke and M. Ernzerhof, *Phys. Rev. Lett.*, 1996, **77**, 3865–3868.
25 J. P. Perdew, K. Burke and M. Ernzerhof, *Phys. Rev. Lett.*, 1997, **78**, 1396.
26 A. Otero-de-la-Roza, M. A. Blanco, A. M. Pendás and V. Luaña, *Comput. Phys. Commun.*, 2009, **180**, 157–166.
27 A. Otero-de-la-Roza, E. R. Johnson and V. Luaña, *Comput. Phys. Commun.*, 2014, **185**, 1007–1018.
28 A. Otero-de-la-Roza and V. Luaña, *J. Chem. Theory Comput.*, 2010, **6**, 3761–3779.
29 G. M. Sheldrick, *Acta Crystallogr. A*, 2008, **64**, 112–122.
30 A. . Volkov, P. Macchi, L. J. Farrugia, C. Gatti, P. Mallinson, T. Richter and T. Koritsanszky, *XD2006 - A Computer Program Package for Multipole Refinement, Topological Analysis of Charge Densities and Evaluation of Intermolecular Energies from Experimental and Theoretical Structure Factors*, 2006.
31 P. J. Becker and P. Coppens, *Acta Crystallogr. A*, 1974, **30**, 129–147.
32 P. J. Becker and P. Coppens, *Acta Crystallogr. A*, 1975, **31**, 417–425.
33 E. D. Stevens and P. Coppens, *Acta Crystallogr. A*, 1976, **32**, 915–917.
34 G. Saleh, L. Lo Presti, C. Gatti and D. Ceresoli, *J. Appl. Crystallogr.*, 2013, **46**, 1513–1517.
35 C. B. Hubschle and P. Luger, *J. Appl. Crystallogr.*, 2006, **39**, 901–904.
36 F. Lihl, *Z. Kristallogr. Krist.*, 1932, **81**, 142–147.
37 K. E. Almin and A. Westgren, *Arkiv Kemi Mineral. Geol.*, 1942, **15**, 1–7.
38 F. Pertlik, *Czech. J. Phys.*, 1978, **28**, 170–176.
39 P. Ballirano and A. Maras, *Z. Kristallogr. NCS*, 2002, **217**, 177–178.
40 Y. A. Abramov, *Acta Crystallogr. A*, 1997, **53**, 264–272.
41 J. Hey, D. Leusser, D. Kratzert, H. Fliegl, J. M. Dieterich, R. A. Mata and D. Stalke, *Phys. Chem. Chem. Phys.*, 2013, **15**, 20600–20610.
42 C. Foroutan-Nejad, S. Shahbazian and R. Marek, *Chem. Eur. J.*, 2014, **20**, 10140–10152.
43 P. A. Guńka, M. Dranka and J. Zachara, *CrystEngComm*, 2011, **13**, 6163–6170.
44 I. D. Brown, *J. Phys. Chem. A*, 2011, **115**, 12638–12645.
45 R. Hoppe and R. Hübenthal, *Z. anorg. allg. Chem.*, 1989, **576**, 169–178.
46 H.-D. Stöver and R. Hoppe, *Z. anorg. allg. Chem.*, 1980, **468**, 137–147.
47 N. Zoche and M. Jansen, *Z. Naturforsch. B*, 1997, **52**, 1031–1036.